Broad iron-Kα emission lines as a diagnostic of black hole spin

Christopher S. Reynolds[1] and Andrew C. Fabian[2]

ABSTRACT

We address the ability of broad iron emission lines from black hole accretion disks to diagnose the spin of the black hole. Using a high-resolution 3-dimensional MHD simulation of a geometrically-thin accretion disk in a Pseudo-Newtonian potential, we show that both the midplane density and the vertical column density of the accretion flow drop dramatically over a narrow range of radii close to the innermost stable circular orbit (ISCO). We argue that this drop of density is accompanied by a sharp increase in the ionization parameter of the X-ray photosphere, and that the resulting imprint of the ISCO on the X-ray reflection spectrum can be used to constrain spin. Motivated by this simulation, we construct a simplified toy-model of the accretion flow within the ISCO of a Kerr black hole, and use this model to estimate the systematic error on inferred black hole spin that may result from slight bleeding of the iron line emission to the region inside of the ISCO. We find that these systematic errors can be significant for slowly spinning black holes but become appreciably smaller as one considers more rapidly rotating black holes.

Subject headings: accretion, accretion disks — black hole physics – galaxies: nuclei – magnetohydrodynamics — relativity

1. Introduction

Recent years have brought an increasing realization of the astrophysical importance of black hole spin. Ever since the seminal work of Penrose (1969) and Blandford & Znajek (1977), it has been recognized that black hole spin may be an important source of energy, especially for the powerful relativistic jets seen emerging from many black hole systems. However, the importance of black hole spin goes beyond its role as a possible power source. The spins of stellar-mass black holes found in accreting Galactic Black Hole Binaries (GBHBs) are expected to be natal (King & Kolb 1999) and give us a window into the black

[1]Dept.of Astronomy, University of Maryland, College Park, MD 20742

[2]Institute of Astronomy, Madingley Road, Cambridge, CB3 OHA, U.K.

hole forming core-collapse supernova. The spin distribution of the supermassive black hole (SMBH) population (and its dependence on SMBH mass) encodes the black hole growth history, e.g., the role of accretion versus mergers (Moderski & Sikora 1996; Volonteri et al. 2005). Thus, across the mass scales, black hole spin gives us a fossil record of how black holes form and grow.

Of course, we must have robust observational probes of black hole spin if we are to truly test spin-powered jet models or actually use spin to probe the formation and growth of black holes. The most direct method imaginable is the characterization of the gravitational radiation emitted as another compact object spirals into the black hole. However, in the current (pre- gravitational wave observatory) era, we must search for signs of black hole spin in the electromagnetic radiation emitted by the surrounding accretion disk. The natural waveband to use is the X-ray band given the fact that the observed X-rays are thought to be predominately emitted from the inner regions of the accretion flow where the relativistic effects related to black hole spin are strongest.

The most important effect of black hole spin on the accretion disk arises from the spin dependence of the location of the innermost stable circular orbit (ISCO); in Boyer-Lindquist coordinates, $r_{\rm isco}$ shrinks from $6GM/c^2$ for a non-rotating black hole down to GM/c^2 for a hole that is maximally rotating in the same sense as the accretion disk. Thus, for a given black hole mass, the characteristic temporal frequency, energy release (and hence temperature), and gravitational redshift of the inner accretion flow all increase as one considers progressively higher black hole spin.

These considerations lead to the three most widely discussed techniques for using X-ray data to determine black hole spin. On the timing front, the frequency stability of the high-frequency quasi-periodic oscillations (HFQPOs) seen in the soft intermediate state of GBHBs strongly suggest a connection to the gravitational potential and black hole spin (Strohmayer 2001; also see McClintock & Remillard [2003] for a general review of HFQPO phenomenology). While HFQPOs may eventually provide a robust way of measuring spins in GBHBs, the lack of a compelling theoretical framework with which to interpret the frequencies prevents any robust conclusions from being drawn at the present time. For example, different and contradictory constraints on the mass and spin of the black hole result from assuming that the HFQPOs are manifestations of trapped global g-modes (Nowak & Wagoner 1992; Nowak et al. 1997), parametric resonances (Abramowicz et al. 2003), or Lens-Thirring precession (Merloni et al. 1999).

The second technique involves modeling the thermal continuum spectrum from the disk. Provided that one selects systems that have optically-thick, geometrically-thin inner accretion disks, observations can be compared with model thermal continuum spectra (which

include vertical radiation transfer in the disk atmosphere as well as Doppler and gravitational red/blue-shifts; Davis, Done & Blaes 2006). Spin results from this technique have been reported by McClintock et al. (2006) and Shafee et al. (2006), although the contrary results of Middleton et al. (2006) demonstrate the current fragility of this technique to modeling the non-thermal emission, particularly when applying it to data from the Proportional Counter Array (PCA) on the *Rossi X-ray Timing Explorer (RXTE)* in which one only sees the Wien tail of the thermal disk spectrum. While this is a powerful method for determining the spin of accreting stellar-mass black holes (especially when applied to broad-band X-ray data that extends into the soft X-ray band), the fact that one needs both an estimate of the black hole mass and a high quality measurement of the thermal continuum shape makes it difficult to apply to the SMBH in active galactic nuclei (AGN). The thermal continuum of AGN disks is in the UV/EUV region of the spectrum, making a determination of its shape and normalization extremely susceptible to any errors in the (large) correction that must be done for dust extinction and photoelectric absorption.

The third technique for constraining spin uses relativistic broadening and gravitational redshifting of the fluorescent iron emission line seen in many GBHBs and AGN (Fabian et al, 1989; Laor 1991; Fabian et al. 2000; Reynolds & Nowak 2003; Fabian & Miniutti 2005). As one considers progressively more rapidly rotating black holes, the primary X-ray emission and hence the iron line emission will be dominated by regions with higher gravitational redshift, leading to broader and more highly skewed iron emission lines. A major advantage of this technique is that the iron line profiles are completely independent of black hole mass and hence one can apply this to an AGN in which the mass is often extremely uncertain. Although one actually proceeds via formal fitting of relativistically smeared theoretical disk reflection spectra to data, the black hole spin constraint essentially results from a characterization of the maximum redshift of the iron line. Results using this technique on the Seyfert galaxy MCG–6-30-15 have been reported by Brenneman & Reynolds (2006) who report rather extreme constraints on the dimensionless black hole spin of $a > 0.987$ (also see Dabrowski et al. 1997).

Both the thermal continuum and the iron line techniques for determining black hole spin rely on the assumption that the ISCO defines an inner edge for the thermally or line emitting region of the disk (see Krolik & Hawley 2002 for a general discussion of the various "inner edges" that one can define for an accretion disk). The robustness of the thermal continuum technique has been explicitly addressed by Shafee, Narayan & McClintock (2007) using a global α-viscosity model that explicitly tracks the flow properties within the ISCO. Although MHD effects close to the ISCO may invalidate the assumptions of such α-models (e.g., Reynolds & Armitage 2001), the results of Shafee et al. (2007) do indeed suggest that modeling of the thermal continuum can produce an accurate measure of black hole spin.

The subject of the current *Paper* is to address the robustness of the iron line fitting technique. In Section 2, we present a high resolution 3-dimensional magnetohydrodynamic (MHD) simulation of a geometrically-thin ($h/r \sim 0.05$) accretion disk that we use to explore the nature of the flow close to the ISCO. In Section 3, we show that both the midplane density and vertically-integrated surface density of the accretion flow drops precipitously over a small range of radii close to the ISCO. We then argue in Section 4 that photoionization of the flow within the ISCO will effectively suppress the iron line emission (and all other X-ray reflection signatures) across most of the region within the ISCO. We discuss the implications and limitations of our results in Section 5, including an estimate of the uncertainties in the inferred black hole spin that might arise from iron line emission in the region immediately within the ISCO. Section 6 presents our conclusions.

2. An MHD simulation of a thin accretion disk

Relativistically broad iron lines are only seen from accretion flows that are relatively cold (i.e., there are recombined iron ions in the plasma) and Compton-thick. Thus, we expect systems displaying broad iron lines to have radiatively-efficient, geometrically-thin accretion disks of the type envisaged by Pringle & Rees (1972), Shakura & Sunyaev (1973) and Nokivov & Thorne (1974).

Our goal is to simulate such an accretion flow in order to assess the nature of the flow around the ISCO. Of course, such black hole accretion disks are very complex systems. It is believed that the underlying angular momentum transport that actually allows accretion to proceed is due to sustained MHD turbulence driven by the magneto-rotational instability (MRI; Balbus & Hawley 1991, 1998). Magnetic energy is dissipated and thermalized through magnetic reconnection on small scales within the body of the disk. In the systems under consideration here, the accretion disk is optically-thick and the resulting thermal radiation comes to dominate the gas pressure and, indeed, provides the principal vertical pressure support for the disk. The radiation diffuses vertically out of the disk and is radiated from the disk atmosphere. Finally, this physics is occurring in a region where both special and general relativistic effects are strong and can have qualitative effects. The most obvious general relativistic effect is the existence of the ISCO. However, frame-dragging, light bending, and the strong displacement currents that accompany the relativistic fluid velocities can all have important effects on disk dynamics (e.g., see fully relativistic MHD simulations of De Villiers et al. 2004, McKinney & Gammie 2004).

Global accretion disk simulations that include all of these physical processes are still beyond current computational capabilities. Moreover, since we are motivated to model

geometrically-thin accretion disks, the need to spatially resolve the vertical structure of the disk while still modeling a significant range of radii imposes severe resolution requirements as will be discussed in more detail below. Clearly, compromises must be made.

These considerations lead us to construct a model of a thin accretion disk employing the simplest possible physics that will enable us to study the structure of the flow around the ISCO. We employ 3-dimensional MHD in order to correctly capture angular momentum transport within the flow due to MRI-driven turbulence. Given that fully relativistic simulation at the required resolution would prove extremely computational intensive, together with the current lack of an adequate publicly available 3-d GRMHD code, we use the Pseudo-Newtonian potential of Pacynski & Witta (1980),

$$\Phi = \frac{GM}{r - 2r_g}, \tag{1}$$

where $r_g = GM/c^2$ is the gravitational radius of the black hole which has mass M. This potential has an ISCO at $r_{\rm isco} = 6r_g$ and, in fact, is a good approximation for the gravitational field of a non-rotating black hole. Although we essentially integrate the equations of non-relativistic MHD within this potential, we use the prescription of Miller & Stone (2000) to include some effects of the displacement current, principally forcing the Alfvén speed to correctly limit to the speed of light as the magnetic fields becomes strong. We note that this "Alfvén speed limiter" only plays a role within the tenuous magnetized atmosphere that forms at large vertical distances above and below the disk; it never plays a significant role in the body of the accretion disk. Furthermore, gas velocities within our simulation are always very subluminal (achieving a maximum of $\sim 0.2c$ at the inner boundary of the simulation domain). Thus, we believe that the neglect of the full set of relativistic terms in the MHD equations should not significantly impact our simulation. We also note that De Villiers & Hawley (2003) explicitly comment upon the similarity of pseudo-Newtonian simulations with full GRMHD simulations performed within a Schwarzschild metric.

In another major simplification, we neglect radiation processes (radiative heating, radiative cooling and radiation pressure). In place of a full energy equation, the gas is given an adiabatic equation of state with $\gamma = 5/3$. Our simulation does not, however, capture the magnetic energy lost to numerical (i.e. grid-scale) reconnection. While not particularly physical, this does acts as an effective cooling term for the disk and helps maintain a thin, cold structure.

The simulation is performed in cylindrical polar coordinates (r, z, ϕ). The initial condition for the simulation consists of a disk with a constant mid-plane density $\rho(r, z = 0) = \rho_0$ for $r > r_{\rm isco}$. The vertical run of initial density and pressure correspond to an isothermal

atmosphere in vertical hydrostatic equilibrium,

$$\rho(r,z) = \rho_0 \exp\left(-\frac{z^2}{2h(r)^2}\right), \tag{2}$$

$$p(r,z) = \frac{GMh(r)^2}{(R-2r_g)^2 R}\,\rho(r,z), \tag{3}$$

where r is the cylindrical radius, z is the vertical height above the disk midplane and $R = \sqrt{r^2+z^2}$. The scale height of the disk as a function of radius is a free function; we choose to set $h(r) = 0.3r_g$ for all r, i.e., a constant height disk with initial $h/r = 0.05$ at the ISCO. The initial density is set to zero for $r < r_{\rm isco}$. The initial velocity field is everywhere set to

$$v_\phi = \frac{\sqrt{GMr}}{r-2}, \qquad v_r = v_z = 0, \tag{4}$$

corresponding to rotation on cylinders and pure Keplerian motion for material on the midplane. An initially weak magnetic field is introduced in the form of poloidal field loops specified in terms of their vector potential $\mathbf{A} = (A_r, A_z, A_\phi)$ in order to ensure that the initial field is divergence free. We choose the explicit form for the vector potential,

$$A_\phi = A_0\, f(r,z)\, p^{1/2} \sin\left(\frac{2\pi r}{5h}\right), \qquad A_r = A_z = 0, \tag{5}$$

where A_0 is a normalization constant and $f(r,z)$ is an envelope function that is unity in the body of the disk and then smoothly goes to zero at both $r = r_{\rm isco}$ and at a location three pressure scale heights away from the midplane of the disk. The use of $f(r,z)$ keeps the initial field configuration well away from either the inner radial boundary of the initial disk configuration or the vertical boundaries of the calculation domain. The final multiplicative term produces field reversals with a radial wavelength of $5h$. This results in a number of distinct poloidal loops throughout the disk and acts as a much more effective seed for the MRI than would a single loop which followed contours of pressure (in the sense that a steady-state is reached more quickly). The normalization constant A_0 is set to give an initial ratio of gas-to-magnetic pressure of $\beta = 10^3$ in the inner disk.

From the body of literature on MRI driven turbulence (e.g., see Balbus 2003), we expect the final turbulent state to be independent of most aspects of the initial field configuration (e.g., see the study of Hawley 2000). In general terms, the one aspect of the initial field that can continue to leave imprints on the turbulent state is the net flux threading the simulation domain (e.g., see Reynolds & Armitage 2001). Our initial condition has zero net flux, a choice that is particularly well defined and robust to implement but is expected to minimize the saturation field strength and the turbulent angular momentum transport. It is beyond

the scope of this paper to explore disks that have a net poloidal field resulting, for example, from advection of magnetic flux from the mass reserviour.

Apart from the Miller & Stone (2000) Alfvén speed limiter, grid effects and the usual artificial viscosity, this simulation deviates from strict ideal MHD in one other way. We impose a floor to the density field of 10^{-5} times the initial maximum density in order to prevent the numerical integration from producing negative densities. This essentially amounts to a subtle distributed mass source. The density only reaches this floor close to the z-boundary (i.e., many scale heights above and below the disk plane).

From these initial conditions, the equations of ideal MHD were evolved using an MPI parallelized version of the ZEUS code (Stone & Norman 1992a,b for a discussion of the basic ZEUS algorithm). The computational domain was the cylindrical wedge defined by $r \in [4, 16]$, $z \in [-1.5, 1.5]$ and $\phi \in [0, \pi/3]$. The computational grid was uniformly spaced in (r, z, ϕ) with $n_r \times n_z \times n_\phi = 480 \times 256 \times 64$. This gridding provides ~ 25 grid cells per vertical pressure scale-height in the body of the disk, adequate to capture the MRI and the large-scale properties of the MHD turbulence that it drives, while also giving a radial grid spacing that is only a factor of two larger than the vertical grid spacing. It is highly desirable to avoid large aspect ratio computational cells due to the anisotropic numerical viscosity and resistivity that it would introduce.

Periodic boundary conditions were imposed on the ϕ-boundaries, and "zero-gradient" outflow boundary conditions were imposed at both the inner and outer radial boundaries (Stone & Norman 1992a,b). The choice of the z-boundary condition is less clear. Experiments employing outflow boundaries in the z-direction showed that tenuous matter generally flows slowly across these boundaries at very sub-sonic and sub-Alfvénic speeds; strictly, this invalidates the use of such boundary conditions (since the flow on the other side of the boundary should be able to act back on the simulation domain). We also note that the use of this outflow boundary condition together with the imposition of the density floor led to occasional numerical instabilities at the z-boundaries (in the form of a small and accelerating magnetized vortex) that, while having no effect on the body of the accretion disk, would eventually halt the simulation. Instead, we choose to employ periodic boundary conditions in the z-directions. While this is obviously unphysical in the sense that matter cannot leave the simulation domain in the vertical direction, it does guarantee mathematically reasonable behaviour at the boundary (eliminating numerical instabilities) and, more importantly, appears to have no effect on the dynamics of the accretion disk itself (as diagnosed through comparisons with our vertical-outflow runs).

The initial state undergoes rapid evolution as radial pressure forces push matter into the (numerical) vacuum within the ISCO. This drives axisymmetric, outward-radially directed

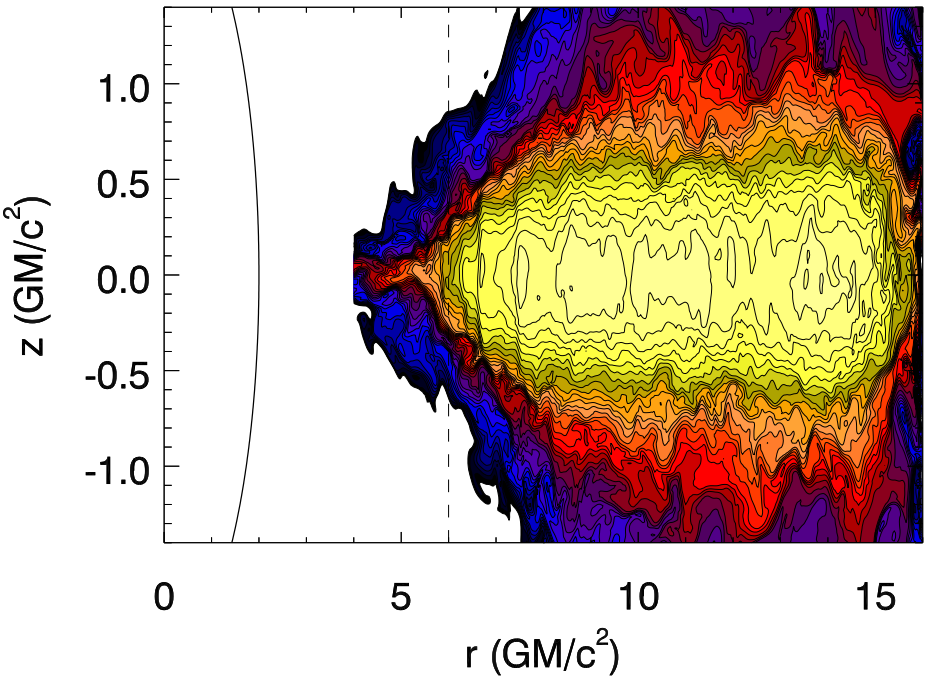

Fig. 1.— Logarithmic density across an azimuthal cross-section of the simulation at time $t = 35T_{\rm isco}$. There are 10 contours per decade of density. The distinct ridges at approximately $6.5r_g$ and $7.5r_g$ are cuts through transient spiral density waves. The simulation domain has an inner radial boundary at $r = 4r_g$. However, the figure shows an extension of this domain to $r = 0$ along with a representation of the event horizon (thick solid black line). Notice the rapid transition of the high density disk into a geometrically-thin, low density accretion stream close to the ISCO.

gravity waves which rapidly break to become outward traveling rolls. These hydrodynamic transients are short lived, lasting for only $5-10T_{\rm isco}$, where $T_{\rm isco} = 61.6GM/c^3$. Concurrently, MRI amplifies the initial magnetic field until the volume-averaged $\beta \sim 50$ at which point the flow becomes turbulent. The simulated disk is turbulent at all radii after $t = 10T_{\rm isco}$. Over the subsequent 7 orbits, the β of the disk declines a little due to the effects of magnetic buoyancy. Examination of the mass accretion rate and total magnetic and thermal energy of the disk show that a quasi-steady state (characterized by approximately constant total magnetic and thermal energies) is achieved after approximately $t = 17T_{\rm isco}$ orbital periods. In this steady state, the dense body of the disk (i.e., close to the mid-plane) is characterized by $\beta \sim 100$. While this is significantly larger than the β found in global simulations of

thicker disk, it is in line with what might be expected for thin accretion disks with zero net field as diagnosed through local shearing-box simulations (Hawley, Gammie & Balbus 1996). We follow the simulation for a total of 40 ISCO orbital periods in order to confirm that it is, indeed, in a quasi-steady state. Figure 1 shows the density of the disk across an azimuthal cross-section at a time $t = 35T_{\rm isco}$.

3. Properties of the flow close to the ISCO

Using this simulation, we can examine the nature of the flow close to the ISCO. Figure 2 (top) shows the mid-plane density and total vertical column density through the disk as a function of r. We see that both the midplane density and total column density undergo a rapid decrease over a small range of radii as the flow crosses the ISCO; the mid-plane density drops by a factor of 20 and the column density drops by a factor of 60 as between $r = 7r_g$ and $r = 5r_g$. Just within the ISCO, the radial scale-length for the mid-plane density and the column density (i.e., the change in radius over which these quantities drop by a factor e) varies from $0.2 - 0.5r_g$, i.e., within a factor of two of the vertical scale-height of the disk outside of the ISCO. In Section 4, we will show that this precipitous drop in density close to the ISCO effectively truncates the iron line emission (i.e., using the terminology of Krolik & Hawley [2002], we argue that the disk has a "reflection edge" that is close to the ISCO).

As expected from simple continuity, this density drop accompanies a rapid increase in the (inward) radial velocity of the gas (bottom panel of Fig. 2). The azimuthally-averaged midplane radial velocity is very close to that of a ballistic infall starting from a circular orbit at $5.7r_g$ (i.e., inset from the ISCO by an amount comparable to the vertical pressure scale-height of the disk just beyond the ISCO). Interestingly, the inflow becomes super-Alfvénic within $r = 5.5r_g$, implying that MHD forces can no longer transport energy and angular momentum upstream within this radius. This is the "stress edge" of the disk, as defined by Krolik & Hawley (2002). The flow is essentially ballistic within this radius. A comparison of this result with those of Hawley & Krolik (2001) supports the conjecture (Armitage, Reynolds & Chiang 2000; Afshordi & Paczynski 2003) that the magnetic extraction of energy and angular momentum from within the ISCO (Krolik 1999; Gammie 1999) becomes less important as one considers progressively thinner accretion disks, at least for the initially zero net-field case.

Another radius of interest is the "turbulence edge", i.e., the radius at which the flow transitions from being a turbulence dominated flow to a more laminar radial inflow. Following Krolik & Hawley (2002), we examine the turbulence edge by comparing the density-weighted azimuthally and vertically-averaged radial velocity $\bar{v_r}$ to the density-weighted root mean

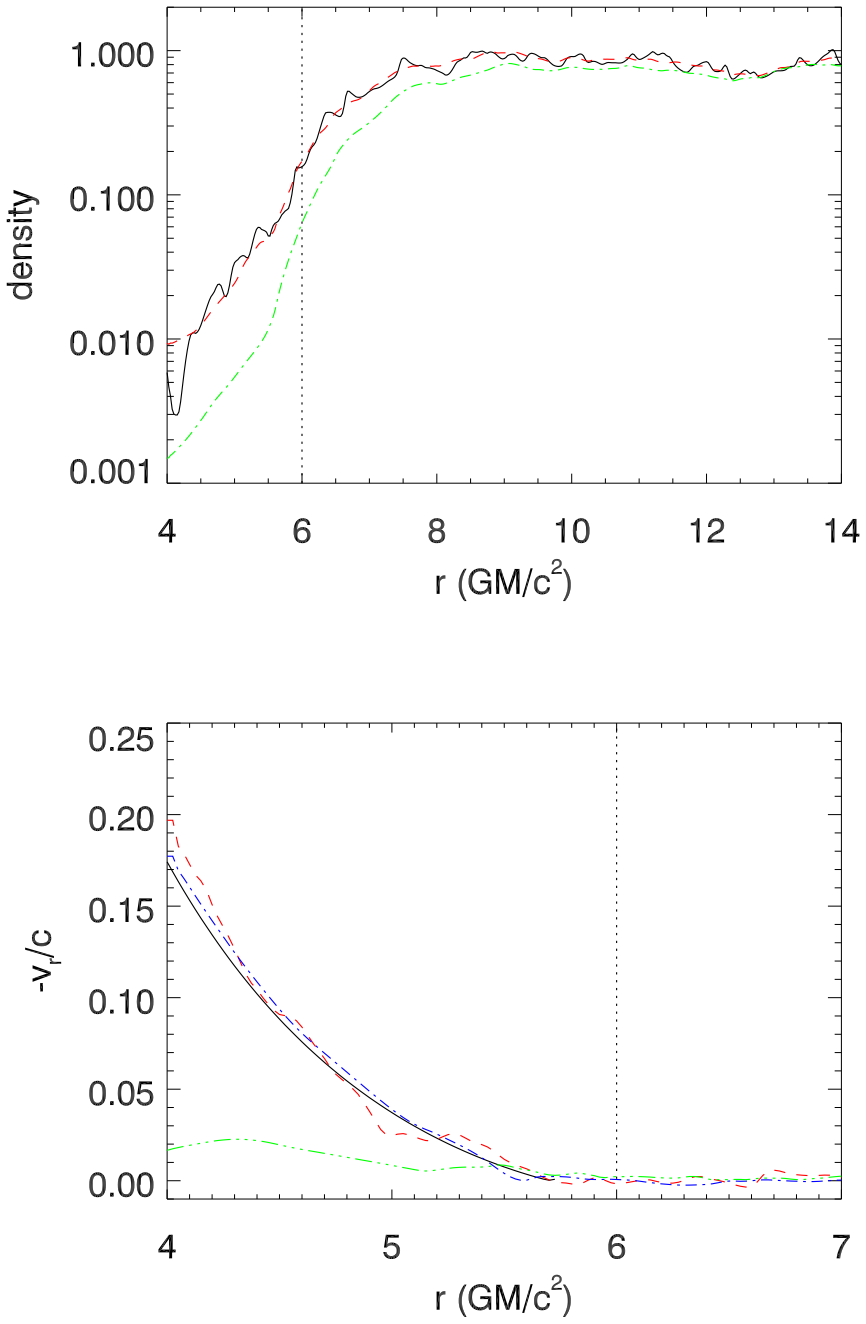

Fig. 2.— *Top panel :* Mid-plane density along a single ray (black solid line), azimuthally-averaged mid-plane density (red dashed line) and (normalized) total vertical column density (green dot-dashed line). The dotted vertical line shows the location of the ISCO. *Bottom panel :* Mid-plane radial velocity along a single ray (red dashed line), azimuthally-averaged mid-plane radial velocity (blue dot-dashed line), and the azimuthally-averaged Alfvén speed (green dot-dashed line). Also shown is the radial velocity of a ballistic trajectory with the energy and angular momentum corresponding to a circular orbit at $5.7r_g$ (solid black line). All quantities are determined at $t = 35T$

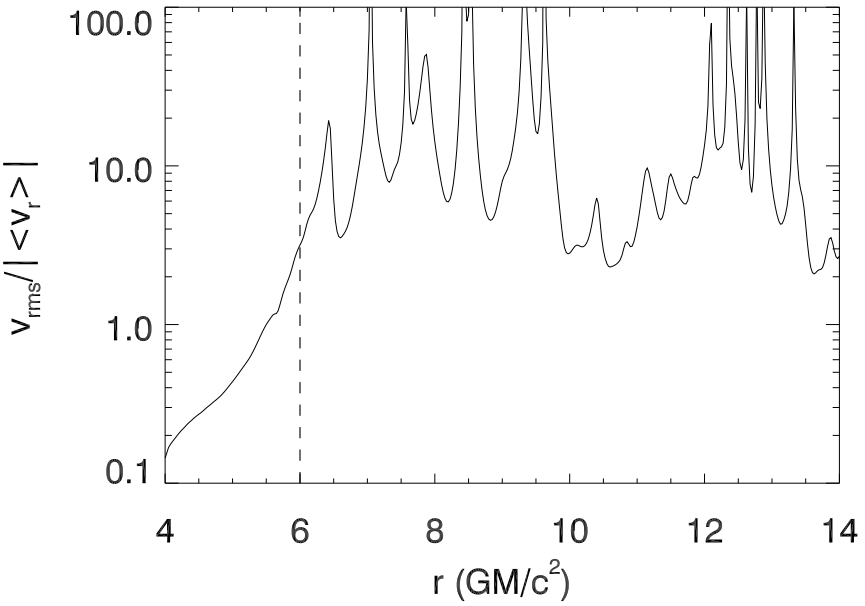

Fig. 3.— Ratio of the density-weighted rms fluctuations of the radial velocity about the (density-weighted) average radial velocity against the average radial velocity. The disk undergoes a transition from a turbulence dominated regime (high values of this ratio) to a more laminar inflow regime (low values of this ratio). The formal "turbulence edge" where this ratio is unity occurs at $r = 5.52r_g$.

square fluctuations of v_r around that average (see Fig. 3). This figure reveals that the disk does not start feeling the effect of the plunging region until $r = 7r_g$, and that the formal turbulence edge at $r \approx 5.5r_g$. Again, we see an abrupt transition close to the ISCO.

We note that the results discussed in this Section appear to be mostly insensitive to the numerical resolution and placement of the vertical boundaries. Re-running the simulation with half the radial and vertical resolution leads to 20–30% increases in the density field and column density within the ISCO, with a comparable decrease in the inflow velocity. A third simulation in which the vertical size of the computational domain is doubled to $z \in [-3, 3]$ (at the reduced resolution) shows essentially identical density and velocity fields both within the disk and inside the ISCO.

4. The use of iron lines as a spin diagnostic

As discussed in the introduction, the current methodology for using broad iron lines to constrain black hole spin relies on the assumption that the iron line emission essentially truncates at the ISCO. Here, we employ our MHD simulation to examine this assumption.

4.1. Physical requirements for iron line production from within the ISCO

The physical requirements for producing significant iron line emission from within the ISCO were first addressed by Reynolds & Begelman (1997; hereafter RB97) using a simple one-zone ballistic model for the accretion flow. There are three principal considerations. Firstly, significant iron line production requires the flow to be Thomson-thick in the vertical direction. For a steadily accreting source with a radiative efficiency η, conservation of baryon number gives the electron scattering optical depth of the plunging region to be,

$$\tau_{\rm e} = \frac{2cr_g}{\eta r(-u^r)}\mathcal{L}, \tag{6}$$

where u^r is the radial component of the 4-velocity, and $\mathcal{L} = L/L_{\rm Edd}$ is the Eddington ratio of the source. Evaluating this at the event horizon of a Schwarzschild black hole (where $u^r \approx -c$ and $r_{\rm h} = 2r_g$), we see that the entire flow within the ISCO is Thomson-thick provided that $L > \eta L_{\rm Edd}$. Using the canonical Schwarzschild value of $\eta \approx 0.06$, we see that the entire flow is optically-thick provided that it is accreting at 6% or more of its Eddington limit, a condition that is very likely satisfied for the active AGN and high-state GBHBs in which we find relativistic broad iron lines. Of course, for more rapidly rotating black holes, the radiative efficiency is higher (achieving a theoretical maximum of $\eta = 0.42$ for a black hole with $a = 1$) leading to the conclusion that the accretion flows around rapidly spinning black holes may have an inner optically-thin region unless the Eddington ratio is close to unity.

The second requirement for significant iron line emission within the ISCO is that this region is irradiated by a hard X-ray source. RB97 adopted the optimal geometry, a hard X-ray source that is located above the black hole, on or close to the symmetry axis of the system. Observational support for just such a geometry has emerged from detailed studies of iron line and reflection bump variability by *XMM-Newton* (Fabian & Vaughan 2003; Miniutti & Fabian 2004) and *Suzaku* (Miniutti et al. 2007).

The third and most constraining requirement is that, despite the irradiation by the hard X-ray source (which may be significantly enhanced by gravitational light-bending) and the plummeting density, the surface layers of the plunging flow must maintain a sufficiently

low ionization state to still produce iron features. RB97 found this to be possible only in the case where a very small fraction of the accretion power ($10^{-3}\dot{M}c^2$ or less) is channeled into the non-thermal X-ray source. Even in this case, the emission line from within the ISCO is mostly from H-like and He-like iron. Young, Ross & Fabian (1998) showed that a significant contribution of such highly ionized iron line emission from within the ISCO would be accompanied by a deep K-shell absorption edge of ionized iron that is absent from the data. Of course, even a fully ionized plunge region will still reflect incident X-ray photons — in this case, the interaction is dominated by Compton scattering and, for X-ray energies under consideration here, the reflected spectrum has the same shape as the incident continuum. When interpreting time-averaged spectra, one could not distinguish between direct primary X-ray emission and primary X-ray emission that has been reflected off the fully ionized flow. However, spectral variability and time-lags might reveal such a component.

4.2. Simulation results

We now reassess the ionization state of the accretion flow within the ISCO, and its ability to produce significant amounts of iron line emission, in the light of the high-resolution MHD simulation presented in Sections 2 and 3. As a preliminary to this discussion, we must dimensionalize our simulation. For an assumed Eddington ratio $\mathcal{L}$, we can apply eqn. 6 to the flow at the inner radial edge of the simulation to relate the (dimensionless) column density in the simulation to the physical column density in the corresponding "real" accretion flow. Further, once the mass M of the central object is chosen, the length and velocity scale of simulation is set, allowing one to dimensionalize the density and pressure.

The X-ray reflection spectrum is sensitive to the ionization state of the matter at the X-ray "photosphere" of the accretion disk, situated approximately at the $\tau_{\rm e} = 1$ surface. For the conditions relevant to these irradiated disk atmospheres, photoionization dominates collisional ionization. Furthermore, the photoionization and recombination timescale of the plasma in both the disk and the plunge region is always very short. Hence, the ionization state of the plasma can be described by an ionization parameter,

$$\xi \equiv \frac{4\pi F_{\rm i}}{n_{\rm ph}}, \tag{7}$$

where $F_{\rm i}$ is the ionizing ($E > 13.6\,{\rm eV}$) radiation flux and $n_{\rm ph}$ is the electron number density of the plasma at the photosphere.

The density and hence ionization state of the plasma at the photosphere will very much depend on the vertical structure of the accretion disk. While we expect our simulation to

capture well the radial angular momentum transport and hence the radial structure of the disk around the ISCO, we are forced to neglect physics that is important for determining the vertical structure. Most importantly, we fail to capture the radiative cooling of the disk material, as well as the role of radiation pressure and radiative transport in the vertical structure. These radiation effects are just recently being included in local (shearing box) simulations of accretion disks (e.g., see Turner 2004; Blaes, Hirose and Krolik 2007) and it is not yet feasible to perform the corresponding global disk simulations. Thus, we must attempt to diagnose the ionization state of the disk atmosphere despite the knowledge that the vertical structure of the simulated atmosphere is incorrect.

We parameterize this uncertainty via the ratio of the density at the photosphere to the average density, $g(r)$, defined by

$$n_{\rm ph} \equiv \frac{\tau_e}{2h\sigma_{\rm T}} g, \tag{8}$$

where h is the scale height defined as the z-value at which the density falls to $1/e$ of its midplane value. We shall refer to $g(r)$ as the *photospheric density parameter*. We expect the radial dependence of τ_e and h close to the ISCO to be determined from the radial dynamics and hence be well described by this simulation. We discuss constraints on $g(r)$ below.

In order to examine the radial run of ionization parameter, we must specify the illuminating ionizing radiation flux as a function of radius. For concreteness (and following RB97), we shall consider a source of ionizing flux situated at a height $D_{\rm s}$ on the z-axis. In the absence of any relativistic effects, the resulting illumination pattern (assuming a flat thin disk) would be

$$F_{\rm i,non-rel} = \frac{L_{\rm i} D_{\rm s}}{(r^2 + D_s^2)^{3/2}}, \tag{9}$$

where $L_{\rm i}$ is the ionizing luminosity of the source. This form is modified due to gravitational light-bending, and the gravitational and Doppler redshifting/blueshifting of source photons (including the k-correction that brings photons into or takes them out of the ionizing regime). For $D_{\rm s} \sim r_{\rm isco}$, the result is to remove the flattening of the illuminating profiles — the resulting profile typically *steepens* from r^{-3} to approximately r^{-4} as one considers smaller and smaller radii (Fukumura & Kazanas 2007).

In what follows, we shall make the conservative assumption that the illumination law maintains a r^{-3} dependence at all radii

$$F_{\rm i} = \frac{L_{\rm i} D_{\rm s}}{4\pi r^3}. \tag{10}$$

This is conservative in the sense that it under-illuminates the innermost regions of the disk (including the region within the ISCO) and hence produces an under-estimate of the

ionization parameter in the plunge region. Thus, the final expression that we use to estimate an ionization parameter from our simulation is

$$\xi = \frac{2L_{\rm i} h D_{\rm s} \sigma_T}{\tau_e r^3} \frac{1}{g}, \tag{11}$$

which, when scaled to typical parameters relevant to a luminous Seyfert galaxy or a high-state GBHB gives,

$$\xi = 1.22 \times 10^2 \left(\frac{h/r}{0.1}\right) \left(\frac{D_s}{r}\right) \left(\frac{\tau_e}{10^3}\right)^{-1} \times \left(\frac{r}{10 r_g}\right)^{-1} \left(\frac{\mathcal{L}_i}{0.01}\right) \frac{1}{g} \ {\rm erg\,cm,s^{-1}} \tag{12}$$

where $\mathcal{L}_i = L_i/L_{\rm Edd}$ is the Eddington ratio for just the ionizing luminosity. Note that eqn. 6 is only strictly meaningful inside the plunge region (where the directed radial inflow exceeds the turbulent fluctuations) and hence it would be inappropriate to use eqn. 6 to simplify eqn. 13.

To demonstrate the problems encountered if we naively adopt the vertical structure of the simulated disk, let us examine the ionization in the disk at $r = 10 r_g$. Observations tell us that these radii in the accretion disks of moderately luminous Seyfert galaxies (with $\mathcal{L} \sim 0.1$ and $\mathcal{L}_i \sim 0.02$) are capable of producing "cold" 6.4 keV iron lines, implying that $\xi < 100$ erg cm, s^{-1}. Employing the $t = 35 T_{\rm isco}$ snapshot, the simulation gives $h/r \approx 0.047$ and, for this Eddington ratio, a total optical depth of $\tau_e \approx 2.5 \times 10^3$. However, integrating a ray into the disk, we hit the $\tau_e = 1$ surface at $z/r \approx 0.14$ giving a photospheric density parameter $g \approx 5.2 \times 10^{-3}$. For $D_s = 6 r_g$, this gives an ionization parameter of $\xi({\rm r} = 10) \approx 5.2 \times 10^3$ erg cm s^{-1}. Such a high ionization parameter would render the disk completely incapable of producing iron line features, contrary to observations. The problem arises due to the low-density, high-temperature atmosphere of gas that envelopes the simulated accretion disk. In real disks, we expect radiative cooling (principally Compton cooling) to collapse this tenuous atmosphere back towards the dense parts of the disk, thereby increasing the plasma density at the photosphere and allowing iron line features to be emitted. The density at the photosphere would be further increased by the action of radiation pressure in the optically-thick body of the disk which tends to flatten the density profile in the optically-thick body of the disk. We can see from the numbers above that the photospheric density parameter must be increased to $g \sim 0.25$ in order to produce the iron line features found in the observations.

In the absence of global simulations that include this physics, we must take a semi-empirical approach. As is clear from above, we need $g \sim 0.1 - 1$ outside of the ISCO in

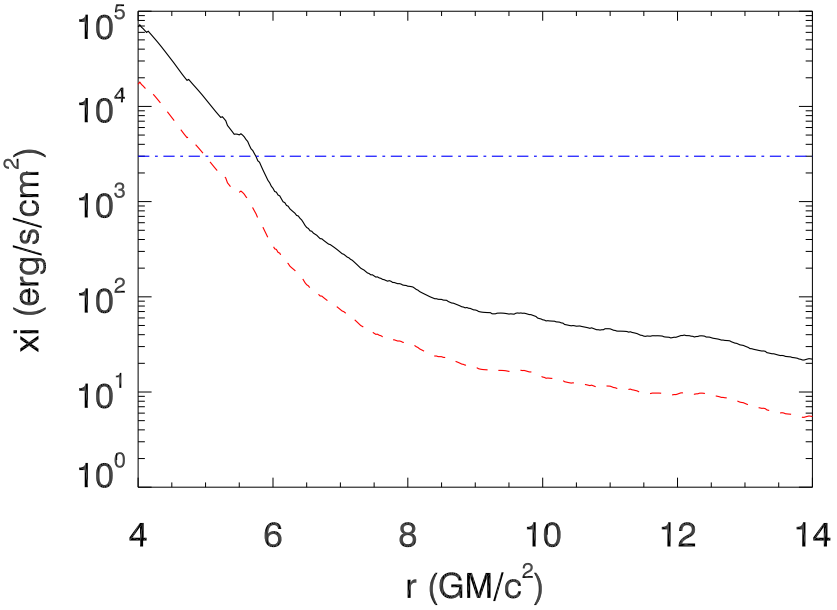

Fig. 4.— Run of photospheric ionization parameter as inferred from the simulation using eqn 13. For all curves shown, $D_s = 6r_g$ and $\mathcal{L}_i/\mathcal{L} = 0.1$. Within this choice of parameters, these curves are valid for all accretion rates. Shown here are the results for $g = 0.25$ (black, solid line) and the extreme case of $g = 1.0$ (red, dashed line). The blue dot-dashed line shows an ionization state of $\xi = 3 \times 10^3$ erg s^{-1} cm^{-2}, above which the production of any iron line emission becomes extremely inefficient. See main text for further details.

order to produce the iron line features that we see in many Seyfert galaxies and high-state GBHBs. We take the approach of assuming that g maintains a constant value of order unity into the plunging region. Figure 4 shows the run of ionization parameter for $g = 0.25$ and the extreme case of $g = 1.0$. Since $\tau_e \propto \mathcal{L}$, eqn. 13 and the curves plotted in Fig. 4 depend only on the fraction of the radiation that is ionizing ($\mathcal{L}_i/\mathcal{L}$) and not the absolute accretion rate or Eddington ratio. Note that the photospheric ionization parameter climbs steeply as one moves inwards into the plunge region. The ionized reflection models of Ross & Fabian (2005) show that distinguishable iron line features are lost when $\xi > 3 \times 10^3$ erg cm s^{-1}. In fact, a deep iron absorption edge (which is not present in the data) accompanies the iron line once $\xi > 1 \times 10^3$ erg cm s^{-1}. Even for the extreme case of $g = 1.0$ (i.e., the photosphere is characterized by the full average density of the disk), the plunge region becomes incapable of producing relevant iron line emission within $5r_g$. For $g = 0.25$, the truncation radius is $5.8r_g$.

5. Discussion

In Section 4, we have demonstrated that the presence of the ISCO leaves a strong imprint on the reflection spectrum of the accretion disk due to the rapid increase in ionization parameter as the flow plunges inwards. The increase in ionization parameter is directly associated with the decrease in both the midplane density and column density of the disk as the flow accelerates inwards. More precisely, for the particular scenario simulated here, we find that the transition in the flow properties occurs on a *radial* length scale which is similar to the *vertical* scaleheight of the disk. Our simulation shows that the azimuthally-averaged midplane radial velocity is very close to that of a ballistic infall starting from a circular orbit at $5.7r_g$ (i.e., inset from the ISCO by an amount comparable to the vertical pressure scale-height of the disk beyond the ISCO). Indeed, our results explicitly demonstrate that the turbulence edge, stress edge, and reflection edge all occur within 2 scaleheights of the ISCO.

Thus, the basic principle underlying the use of broad iron lines as a spin diagnostic is validated. However, it should also be apparent that the iron line emission may not truncate *precisely* at the ISCO. Thus, we must expect to introduce a systematic error in the black hole spin when we fit observational data with models that do truncate precisely at the ISCO. A detailed quantification of these systematic errors would involve fitting ISCO-truncated iron line profiles to realistic synthetic data that have been produced from models that include some contribution from within the ISCO. Here, we address this issue using a simpler (if somewhat less constraining) approach based on the maximum observed redshift of the iron line features.

Motivated by our simulation, we consider the following (relativistic) toy-model for the plunge region of an accretion disk around a rotating black hole. We consider an accretion disk whose mid-plane lies in the equatorial plane of a Kerr spacetime with dimensionless spin parameter a. We suppose that the disk has a vertical scale-height of h just outside of the ISCO; h and a are considered parameters of this toy-model. We assume that the accreting matter follows circular test-particle orbits within the Kerr spacetime down to a radius $r = r_{\rm plunge}$. Motivated by our MHD simulation above, we suppose that $r = r_{\rm plunge}$ is located a proper radial distance h inside the ISCO of the Kerr black hole (as measured by an observer orbiting with the flow at $r = r_{\rm plunge}$). The flow within $r = r_{\rm plunge}$ is assumed to follow ballistic trajectories with the specific energy and specific angular momentum of the circular flow at $r = r_{\rm plunge}$. Thus the velocity field of the accretion flow is defined once we specify h and a. See the Appendix of Reynolds et al. (1999) for a summary of the relativistic expressions used to compute this velocity field.

We assume that there is a source of ionizing radiation situated on the spin axis of the

black hole at a height $D_s = r_{\rm isco}$. Given the velocity field for the accretion flow described above, we can combine the conservation of baryon number (eqn. 6) and the relation between ionization parameter and vertical optical depth (eqn. 11) in order to deduce that

$$\xi = \frac{4\pi D_s \eta_{\rm ion} m_p c^2 (-u^r)}{gr} \left(\frac{h}{r}\right)_{\rm pl}, \tag{13}$$

where $\eta_{\rm ion}$ is the efficiency with which the rest mass of the accretion flow is converted into *ionizing* luminosity of the source. Then, for assumed values of D_s, $\eta_{\rm ion}$, g and (h/r), we can estimate the radius in the accretion flow becomes too highly ionized to produce significant iron line emission. We set this limiting ionization parameter to be $\xi = 3000\,{\rm erg\,cm\,s^{-1}}$.

Suppose that one is attempting to constrain the spin of the black hole through the maximum redshift of the iron line. If the true spin of the black hole is $a_{\rm real}$, we use the above toy-model to determine the innermost radius that contributes to the observable iron line emission. Hence, the observed iron line feature will be more highly redshifted than if it were truncated at the ISCO. We use the algorithms and subroutines of Roland Speith (Speith, Riffert & Ruder 1995) to compute the maximum observed redshift of this iron feature. We then determine the black hole spin $a_{\rm fit}$ for which the same maximum redshift would be obtained if the iron line emitting region is strictly truncated at the ISCO.

Figure 5 shows the results of this exercise; the difference between $a_{\rm fit}$ and $a_{\rm true}$ in these plots indicates the degree to which the black hole spin can be overestimated due to the effects of unmodelled iron line emission within the plunge region. In generating these figures, we have assumed the canonical value of the photospheric density parameter $g = 0.25$ and a source which is at $D_s = r_{\rm isco}$. Motivated by our simulations, we also assume that the flow within the plunge region has collapsed in the vertical direction such that $h/r = 0.01$. Finally, we assume that the total radiative efficiency of the flow is that of a standard Novikov & Thorne (1974) accretion disk, and that 20% of this luminosity is release in the form of ionizing luminosity from the on-axis source. This last assumption is probably conservative and motivated by the multiwaveband observation of the prototypical source MCG–6-30-15 which shows that *at least* 20% of the accretion luminosity is radiated into the highly-variable X-ray/γ-ray tail (Reynolds et al. 1997).

There are several noteworthy aspects of the results reported in Fig. 5. Firstly, the uncertainty in the black hole spin parameter introduced by bleeding of the iron line emission region within the ISCO is generally more important for slowly spinning black holes. This is directly related to the fact that both the spacetime metric and the properties of the accretion disk are slowly varying functions of black hole spin when $|a| \ll 1$; hence a significant change in black hole spin is required if an ISCO-truncated iron line is to mimick the additional redshift introduced by the bleeding of the line emission region within the ISCO.

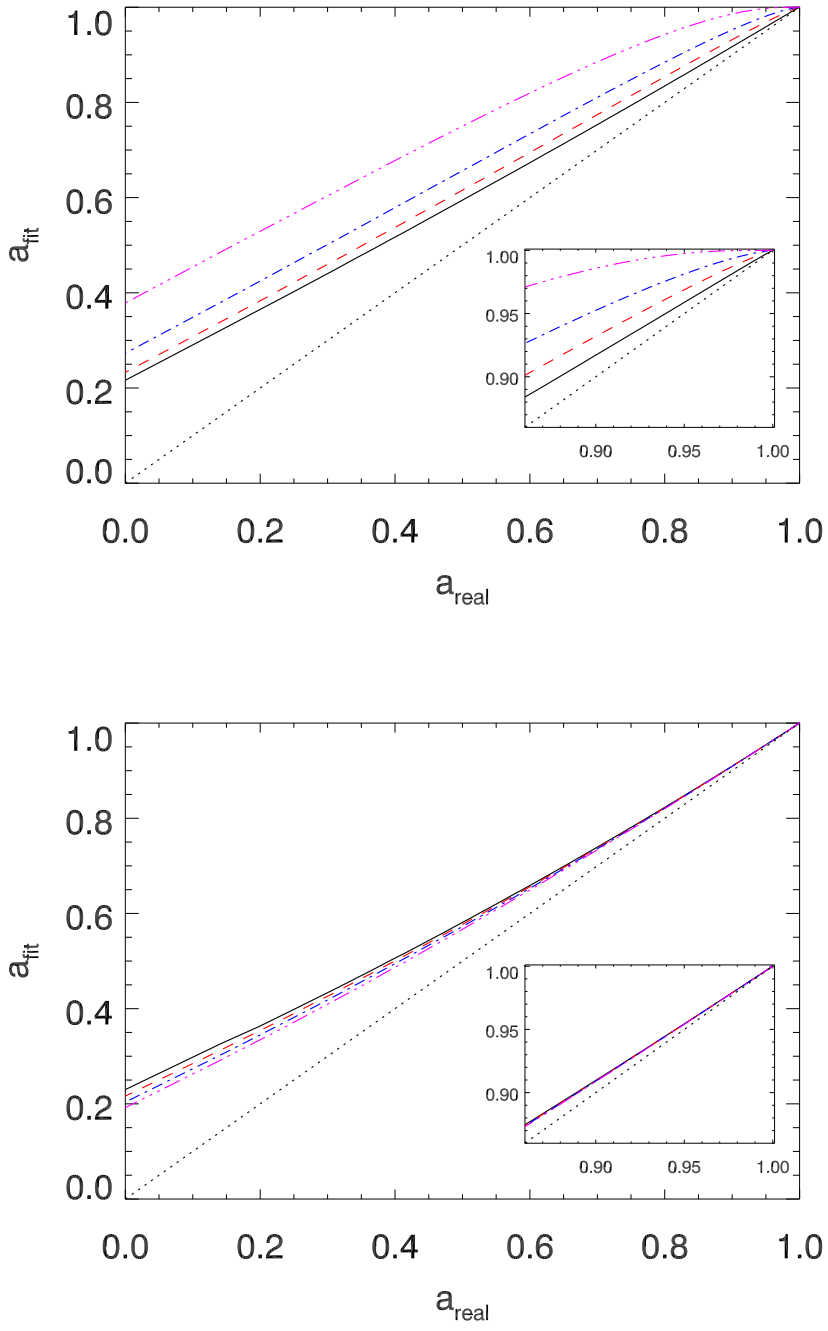

Fig. 5.— Inferred spin value $a_{\rm fit}$ as a function of actual spin $a_{\rm real}$ using the maximum redshift method described in the text; here we assume $g = 0.25$, $D_s = r_{\rm isco}$, $(h/r)_{\rm pl} = 0.01$. We also assume that the accretion flow has the standard radiative efficiency of a Novikov & Thorne (1974) accretion disk, and that 20% of that luminosity is in the form of ionizing radiation. The *top panel* shows the effect of varying the vertical scale height of the disk just outside of the ISCO; an inclination of $i = 30°$ is assumed and lines show the very thin case $h = 0.01$ (solid black line), $h = 0.25r_g$ (red dashed line), $h = 0.5r_g$ (dot-dashed blue line), and $h = 1.0r_g$ (dot-dot-dot-dashed blue line). The *bottom panel* demonstrates that the viewing

Secondly, the systematic error on the black hole spin increases as one considers accretion disks that have greater vertical scale height just outside of the ISCO. Even for $h \sim r_g$, however, one will still clearly distinguish rapidly spinning black holes ($a > 0.8$) from slowly spinning holes. Future global simulations of radiative and radiation-pressure dominated accretion disks will be required in order to assess the realistic range of disk thicknesses that characterize broad iron line sources. We do note, however, that current observations impose an important constraint on the geometric thickness of the inner disk in broad iron line Seyfert galaxies and GBHBs. For example, spectral modeling of MCG–6-30-15 shows the inner accretion disk to have a (photospheric) ionization parameter of $\xi \sim 100\,\mathrm{erg\,cm\,s^{-1}}$ (Brenneman & Reynolds 2006). Using eqn 13 with canonical parameters discussed in Section 4.2 ($\tau \approx 10^3$, $\mathcal{L}_i = 0.02$, $D_s \approx 6r_g$), we see that this measured ionization parameter along with the condition $g < 1$ demands that $h < 0.6r_g$ at $r = 6_g$, and $h < 0.1r_g$ at $r = 3_g$. Of course, a more rigorous exploration of this toy-model, employing relativistically correct treatments of the ionizing irradiation (beyond the scope of this paper), is required to obtain reliable limits on the disk thickness for rapidly rotating black holes.

Thirdly, the precise inclination of the accretion disk has a very weak effect on the systematic error on the black hole spin (as long as the inclination is known from, for example, modeling of the overall broad iron line profile).

Our results suggest that the true spin and the inferred spin become much closer as one considers more rapidly rotating black holes. Of course, for extreme spin values, the inner emitting part of the disk is very close to the event horizon and well within the ergosphere of the black hole. Interactions of the (magnetized) accretion flow with the strong frame-dragging will likely invalidate the assumptions of the toy-model presented here. Significant further work using fully relativistic codes to explore thin accretion disks is required in order to assess whether the picture of a well defined transition in flow properties around the ISCO makes sense for such rapidly rotating black holes.

6. Conclusions

It is a fundamental fact that one can, in principle, observe arbitrarily large gravitational redshifts from around any black hole, irrespective of its spin parameter. Indeed this is very closely tied to the definition of a black hole. At first glance, this fact would appear to render impotent attempts to determine spin using the gravitational redshift of iron emission lines. However, it is the *astrophysics* of black holes accretion and the change in the character of the flow around the ISCO that gives observations of broad iron lines (and X-ray reflection in general) the power to diagnose black hole spin.

To understand the behavior of the accretion flow close to the ISCO, one must capture the angular momentum transport as fully as possible. Models based on parameterized anomalous viscosity (e.g., α-models) can become acausal within the plunge region and cannot capture the non-local MHD stresses that may operate around the ISCO. Fully 3-d MHD simulations provide the most powerful tool to examine these complex flows. All previously published global 3-d MHD simulations of black hole accretion disks have revealed rather gradual transitions of flow properties around the ISCO, but have modeled rather thick ($h/r \sim 0.1$ or greater) accretion flows.

Motivated by the fact that luminous Seyfert nuclei and high-state GBHBs (i.e., the systems in which we actually observe broad iron lines) are thought to possess geometrically-thin disks, we have examined the nature of the flow around the ISCO using a high-resolution pseudo-Newtonian MHD simulation of a disk with $h/r \sim 0.05$. We find a rather abrupt transition of flow properties across the ISCO; the radial length-scale of these changes is comparable to the vertical scaleheight of the disk beyond the ISCO. In the language of Krolik & Hawley (2002), the "stress edge" and the "turbulence edge" of the disk are at $r \approx 5.5r_g$ compared with $r_{\rm isco} = 6r_g$. Most importantly for the present discussion, we find that both the midplane density and column density of the disk drop dramatically as the flow accelerates inwards. Although there is no radiation in the simulation, we relate the simulation quantities to the expected ionization state of the accretion flow and find that (even under conservative assumptions aimed at minimizing the ionization state of the plunging flow) significant iron line emission cannot be produced from inside $r = 5r_g$. In fact, for canonical parameters, this "reflection edge" is at $r \approx 5.8r_g$, very close to the ISCO.

The fact that the iron line emission does not truncate precisely at the ISCO will, however, introduce a systematic error into iron line based spin measurements that assume strictly ISCO-truncated line profiles. We make a first attempt to quantify this systematic error in Section 5, although we note that this approach neglects the spin information which is carried by the full line profile (as opposed to just the maximum redshift). Further study is required to assess whether, in practice, the information carried by the full line profile dramatically decreases the systematic error estimates of Fig. 5.

We thank Laura Brenneman, Eve Ostriker, Cole Miller, Jon Miller and John Vernaleo for stimulating discussion related to this project. We also thank the anonymous referee for insightful and courteous comments. All simulations described in this paper were performed on the Beowulf cluster ("The Borg") supported by the Center for Theory and Computation (CTC) in the Department of Astronomy at the University of Maryland College Park. CSR gratefully acknowledges support from the National Science Foundation under grant AST 06-07428, and the University of Maryland under the Graduate Research Board Semester Award

Program. ACF thanks the Royal Society for support.

REFERENCES

Abramowicz M.A., Karas V., Kluzniak W., Lee W.H., Rebusco P., 2003, PASJ, 55, 467

Afshordi N., Paczynski B., 2003, ApJ, 592, 354

Armitage P.J., Reynolds C.S., Chiang J., 2001, ApJ, 548, 868

Balbus S.A., 2003, ARA&A, 41, 555

Balbus S.A., Hawley J.F., 1991, ApJ, 376, 214

Balbus S.A., Hawley J.F., 1998, Rev. Mod. Phys., 70, 1

Blaes O., Hirose S., Krolik J.H., 2007, ApJ, in press (astro-ph/0705.0314)

Blandford R.D., Znajek R.L., 1977, MNRAS, 179, 433 (BZ)

Brenneman L.W., Reynolds C.S., 2006, ApJ, 652, 1028

Dabrowski Y., Fabian A.C., Iwasawa K., Lasenby A.N., Reynolds C.S., 1997, MNRAS, 288, L11

Davis S.W., Done C., Blaes O.M., 2006, ApJ, 647, 525

De Villiers, J.P., Hawley J.F., 2003, ApJ, 589, 458

De Villiers, J.P., Hawley J.F., Krolik J.H., Hirose S., 2005, ApJ, 620, 878

Fabian A.C., Vaughan S., 2003, MNRAS, 340, L28

Fabian A.C., Miniutti G., 2005, astroph/0507409

Fabian A.C. et al., 1989, MNRAS, 238, 729

Fabian A.C., Iwasawa K., Reynolds C.S., Young A.J., 2000, PASJ, 112, 1145

Fukumura K., Kazanas D., 2007, ApJ, in press (astro=ph/0704.2159)

Gammie C.F., 1999, ApJ, 522, L57

King A.R., Kolb U., 1999, MNRAS, 305, 654

Krolik J.H., 1999, ApJ, 515, L73

Krolik J.H., Hawley J.F., 2002, ApJ, 573, 754

Hawley J.F., 2000, ApJ, 528, 462

Hawley J.F. Krolik J.H, 2001, ApJ, 548, 348

Hawley J.F., Gammie C.F., Balbus S.A., 1996, ApJ, 464, 690

Laor A., 1991, ApJ, 376, 90

McClintock J.E., Remillard R.A., 2003, astroph/0306213

McClintock J.E., Shafee R., Narayan R., Remillard R.A., David S.W., Li L.-X., 2006, ApJ, 652, 518

McKinney J.C., Gammie C.F., 2004, ApJ, 611, 977

Merloni A., Vietri M., Stella L., Bini D., 1999, MNRAS, 304, 155

Middleton M., Done C., Gierlinski M., Davis S.W., 2006, MNRAS, 373, 1004

Miller K.A., Stone J.M., 2000, ApJ, 534, 398

Miniutti G., Fabian A.C., 2004, MNRAS, 349, 1435

Miniutti G. et al., 2007, PASJ, 59, 315

Moderski R., Sikora M., 1996, MNRAS, 283, 854

Nowak M.A., Wagoner R.V., 1992, ApJ, 393, 697

Nowak M.A., Wagoner R.V., Begelman M.C., Lehr D., 1997, ApJL, 477, L91

Novikov, I., Thorne K.S., 1973, in Black Holes, 1973, ed. C.DeWitt and B.DeWitt(New York: Gordon and Breach).

Paczynski B., Wiita P.J., 1980, A&A, 88, 23

Penrose R., 1969, Riv. de Nuovo Cim., 1, 252

Pringle J.E., Rees M.J., 1972, A&A, 21, 1

Reynolds C.S., Armitage P.J., 2001, ApJL, 561, L81

Reynolds C.S., Begelman M.C., 1997, ApJ, 488, 109 (RB97)

Reynolds C.S., Ward M.J., Fabian A.C., Celotti A., 1997, MNRAS, 291, 403

Reynolds C.S., Nowak M.A., 2003, Phys. Reports, 377, 389

Ross R.R., Fabian A.C., 2005, MNRAS, 358, 211

Shafee R., Narayan R., McClintock J.E., 2007, ApJ, submitted (astro-ph/0705.2244)

Shafee R., McClintock J.E., Narayan R., Davis S.W., Li L.-X., Remillard R.A., 2006, ApJ, 636, L133

Shakura, N.I., Sunyaev, R.A., 1973, A&A, 24,337

Speith R., Riffert H., Ruder H, 1995, Comput. Phys. Commun., 88, 109

Strohmayer T.E., 2001, ApJ, 552, L49

Stone J.M., Norman M.L., 1992a, ApJS, 80, 753

Stone J.M., Norman M.L., 1992b, ApJS, 80, 791

Turner N.J., 2004, ApJ, 605, L45

Volonteri M. et al., 2005, ApJ, 620, 69

Young A.J., Ross R.R., Fabian A.C., 1998, MNRAS, 300, L11